Crossover in the dynamics of cell wall growth controls *Caulobacter* division times

Shiladitya Banerjee,[1,2,3] Klevin Lo,[1,4] Alan Selewa,[4,5] Thomas Kuntz,[6]
Matthew K. Daddysman,[4] Aaron R. Dinner,[1,4,6,*] and Norbert F. Scherer[1,4,6,*]

[1] *James Franck Institute, The University of Chicago, Chicago IL 60637, USA*

[2] *Department of Physics and Astronomy,*
University College London, London WC1E 6BT, UK

[3] *Institute for the Physics of Living Systems,*
University College London, London WC1E 6BT, UK

[4] *Institute for Biophysical Dynamics, The University of Chicago, Chicago IL 60637, USA*

[5] *Biophysical Sciences Graduate Program,*
The University of Chicago, Chicago IL 60637, USA

[6] *Department of Chemistry, The University of Chicago, Chicago IL 60637, USA*

[*] To whom correspondence may be addressed. Email: dinner@uchicago.edu or nfschere@uchicago.edu.

Cell size is specific to each species and impacts their ability to function. While various phenomenological models for cell size regulation have been proposed, recent work in bacteria have demonstrated an *adder* mechanism, in which a cell increments its size by a constant amount between each division. However, the coupling between cell size, shape and constriction, remain poorly understood. Here, we investigate size control and the cell cycle dependence of bacterial growth, using multigenerational cell growth and shape data for single *Caulobacter crescentus* cells. Our analysis reveals a biphasic growth mechanism: a relative *timer* phase before constriction where cell growth is correlated to its initial size, followed by a pure *adder* phase during constriction. Cell wall labeling measurements reinforce this biphasic behavior: a crossover from uniform lateral growth to localized septal growth is observed. We develop a mathematical model that quantitatively explains this *mixer* mechanism for size control.

We recently introduced a technology that enables obtaining unprecedented amounts of precise quantitative information about the shapes of single bacteria as they grow and divide under non-crowding and controllable environmental conditions [1, 2]. Others have developed complementary methods [3–6]. These single-cell studies are generating great interest because they reveal unanticipated relationships between cell size and division control [5]. Recent work in bacteria that utilize these technologies revealed that a constant size increment between successive generations [7] quantitatively describes the strategy for bacterial size maintenance in *E. coli* [3–5], *B. subtilis* [5], *C. crescentus* [4], *P. aeruginosa* [8] and even in the yeast *S. cerevisiae* [9]. This phenomenological observation has been termed an *adder* model for cell size control. Competing models for size control include cell division at a critical size (*sizer* model) [10] or at a constant interdivision time (*timer* model) [1]. Analysis of single-cell data show that cell size at division is positively correlated with the cell size at birth [1, 4, 5, 11, 12], thus precluding a sizer model. In addition, a negative correlation between initial cell size and interdivision times, as reported here and in refs [1, 4, 5, 12, 13], is inconsistent with the timer model. However, other studies have suggested mixed models of size control, with diverse combinations of sizer, timer and adder mechanisms [14–17]. The spatial resolution and statistically large size of our data now allow us to revisit these issues with greater precision.

While cell size serves as an important determinant of growth, the bacterial cell cycle is composed of various coupled processes including DNA replication and cell wall constriction that have to be

faithfully coordinated for cells to successfully divide [18]. This raises the question of what other cell cycle variables regulate growth and how the interplay between these different coupled variables can be understood quantitatively [19, 20]. Indeed, our recent analysis of cell shapes revealed how different cell shape variables are coupled through growth and division [2]. Our shape analysis further led to the development of a general physical theory for cell shape dynamics [21], which provides testable quantitative predictions for the interplay between cell shape, growth and division control.

Here we transcend our previous works by relating the mechanism of cell size control and cell wall growth to the timing of cell-wall constriction in *C. crescentus* cells. Our experimental data and analysis reveal that *C. crescentus* cell growth is correlated to its initial size prior to constriction (a *relative timer* mechanism), and adds a constant size during cell-wall constriction leading to the formation of daughter cell poles (an *adder* mechanism). Furthermore, the onset of constriction occurs at a fixed phase of the cell cycle, but is uncorrelated to the cell size at birth. We term this biphasic size regulation behavior a *mixer* mechanism for cell size control, and we find it to be operative over the range of physiologically relevant temperatures of the organism. Furthermore, by fluorescently labeling the cell walls of a synchronized population of *C. crescentus* cells and analyzing the resultant spatial profiles, we find a crossover in cell wall growth dynamics from uniform lateral growth to localized septal growth at the onset of cell wall constriction; that is, a crossover from a timer to an adder mechanism. This finding motivates our development of a mathematical model of the physical origin of cell size control that faithfully captures the aforementioned new experimental pheonomenology.

RESULTS

We use a combination of microfluidics and phase-contrast microscopy for high-throughput, live-cell measurements of cell shape dynamics of single *C. crescentus* cells [1, 2, 22] (see Supplementary Methods). As a population of cells is controllably attached via a stalk and holdfast to the coverslip surface in the microfluidic channel, our measurements allow obtaining accurate and precise data of single cell shape and growth for >10000 generations for >250 cells under steady environmental conditions. From the splined cell contours of the acquired phase-contrast images (Fig. 1A), we determine various cell shape parameters, such as the length of the cell midline axis (l), the width of the cell, and also the radius of curvature of the midline. As reported previously, the length (l) increases exponentially with time constant $\langle\kappa\rangle^{-1} = 125 \pm 8$ min and a mean division time

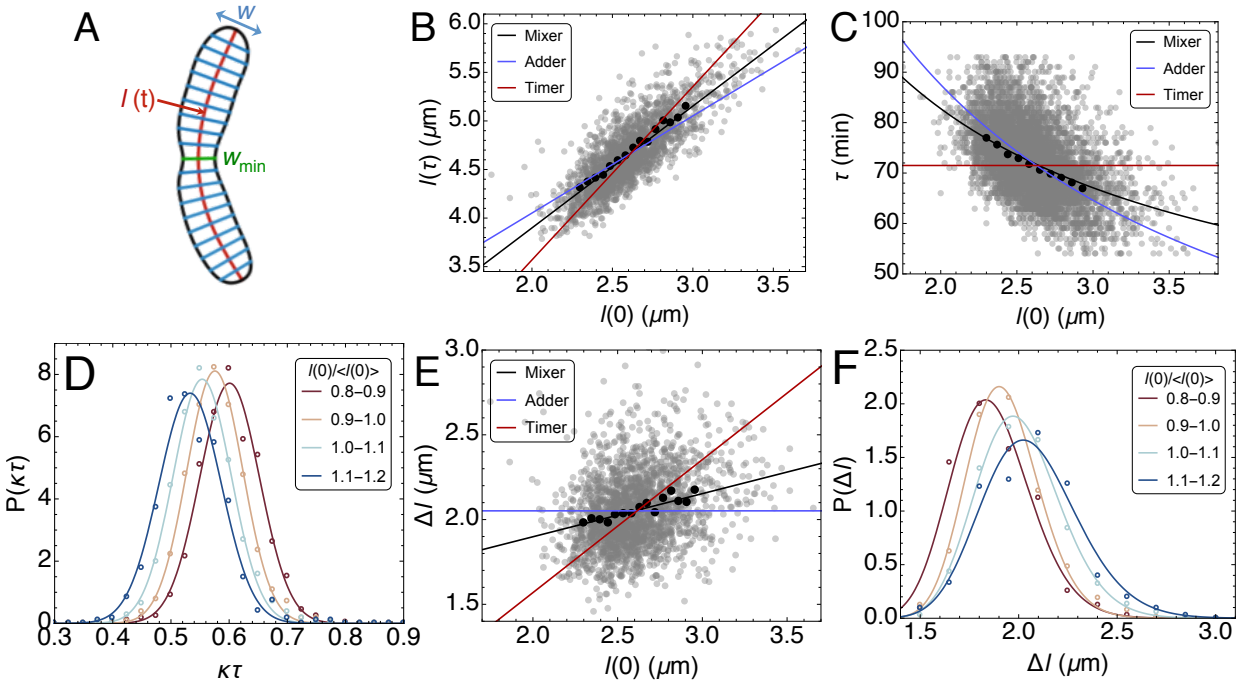

FIG. 1. **Cell size and division control in *C. crescentus* cells**. (A) A representative splined contour of a *C. crescentus* cell, illustrating the shape variables. (B) Cell size at division, $l(\tau)$, vs the cell size at birth, $l(0)$. The black solid line represents a least square linear fit to all single generation data given by the gray scatter cloud (mixer model). Corresponding fits by timer and adder models are given by red and blue lines, respectively. The solid circles represent mean data binned by $l(0)$. (C) The scatter plot of interdivision times, τ, vs the initial cell size, $l(0)$, exhibits a negative correlation. The black solid line is the prediction from our exponential growth and mixer model with no adjustable fitting parameters. Predictions from timer and adder models are shown by the red and blue lines. (D) The conditional probability density of normalized cell cycle time, $\kappa\tau$, given the mean rescaled initial length values, $P(\kappa\tau|l(0)/\langle l(0)\rangle)$, illustrating the negative feedback between τ and $l(0)$. The open circles represent experimental data and the solid curves are Gaussian fits. (E) Size extension in each generation, Δl is correlated with the initial cell size. The mean trend is described by the linear relationship, $\Delta l = (a-1)l(0) + \delta$, which is the mixer model. (F) shows the conditional probability density of size extension Δl given the mean rescaled initial cell length, $P(\Delta l|l(0)/\langle l(0)\rangle)$. The open circles represent experimental data and the solid curves are lognormal fits.

$\langle\tau\rangle = 73 \pm 7$ min at 31°C (in peptone-yeast extract medium), while the average width and the radius of curvature remains approximately constant [2]. Since measurements of the cell area behave the same as the length [1], we use the length of the midline axis of the cell, l, as a metric for cell size.

Mixer model of cell size control. We first analyzed the correlation between cell size at birth, $l(0)$, and the cell size at division, $l(\tau)$, since it reflects the intergenerational strategy for cell size

control. While we previously considered only pure timer ($l(\tau) = al(0)$) and adder ($l(\tau) = l(0) + \delta$) models [1], here, consistent with [16], we find that the final cell size can best be described by a model that combines them: $l(\tau) = al(0) + \delta$, with a slope of $a = 1.25$ and an intercept $\delta = 1.39$ μm (Fig. 1B; Supplementary Information; Supplementary Figure 1). The value of the slope should be compared with 1.8, the multiple expected for a mean division ratio of $\simeq 0.55$ between the daughter cells. Since the cells grow at a constant exponential growth rate, κ, the non-zero positive value of the intercept δ implies that larger cells divide at a shorter time and vice-versa [4, 5, 7, 12],

$$\tau = \kappa^{-1} \ln \left[a + \delta / l(0) \right] . \tag{1}$$

In agreement with previous reports [4], we find the interdivision times, τ, to be negatively correlated with the initial cell lengths (Eq. (1); Fig. 1C). In addition, as shown in Fig. 1D, the distribution of normalized cell cycle times, $\kappa\tau$, are also correlated with the initial lengths as shown by the conditional probability $P(\kappa\tau | l(0)/\langle l(0) \rangle)$ for various ranges of $l(0)/\langle l(0) \rangle$. These observations rule out a pure timer mechanism of cell size control where the division times would be uncorrelated with the initial lengths. Furthermore, Figures 1E and F show that the lengths added in each generation, $\Delta l = l(\tau) - l(0)$, are positively correlated with the initial cell lengths, which precludes a pure adder model for cell size control, in contrast to [4]. We note that the probability densities for $\kappa\tau$ are well-approximated by a Gaussian, indicating that the intergenerational noise may be additive in $\kappa\tau$, which is consistent with the log-normal distributions of the additive size [7].

Our experiments thus suggest that *C. crescentus* cells behave as a *mixer*, with both timer and adder components. Furthermore, we find that this mixer mechanism is conserved in the temperature range 14°C-34°C (Supplementary Figures 2,3). Interestingly cells at 37°C behave as a perfect adder, which suggests that adder-like behavior may be elicited by experimental conditions. For *C. crescentus*, 37°C is the extreme upper limit for viable cell growth.

Crossover in cell wall growth dynamics. Since a mixer model implements a timer ($al(0)$) and an adder component (δ) serially, we conducted new experiments to determine if we can visualize a crossover from timer to adder behavior in the cell cycle. We sought to examine the cell cycle dependence of peptidoglycan synthesis, by using a fluorescent construct of lectin wheat germ agglutinin (flWGA) that labels the cell wall of Gram-negative *C. crescentus* cells [23]. Using the microfluidics platform we previously developed [1], *C. crescentus* cells were initially incubated in media with PYE and flWGA for 15 minutes without flow, allowing the cells to be covered with flWGA (see Supplementary Methods). PYE media were then flowed into the microfludics

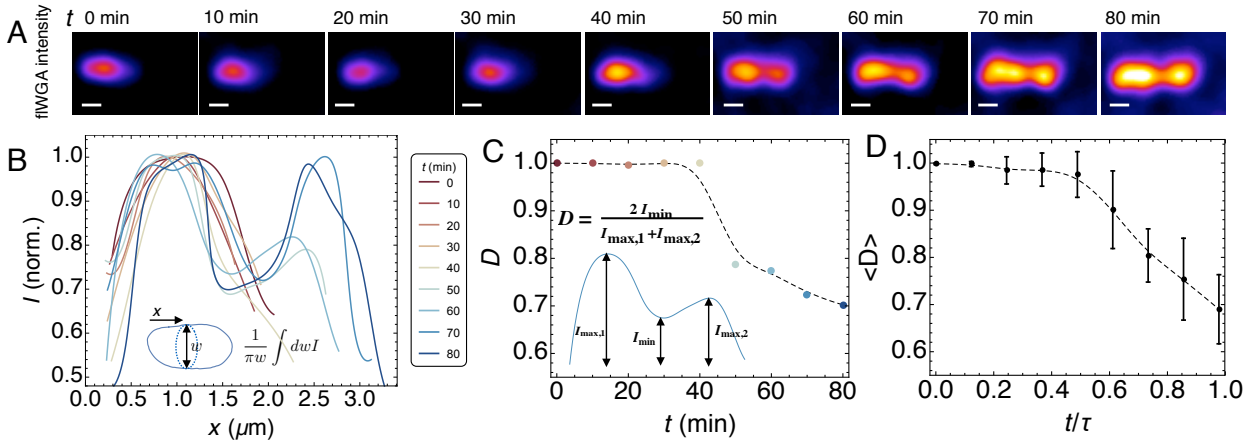

FIG. 2. **Crossover in cell wall growth dynamics at the onset of constriction**. (A) Confocal fluorescent images of *C. crescentus* cells in a microfluidic flow cell labeled with fluorescent WGA taken after 0, 10, 20, 30, 40, 50, 60, 70 and 80 min of growth in PYE medium. The images are deconvoluted using the Huygens software package (see Supplementary Methods). The scale bars represent 0.7 μm. The depletion of fluorescence reveals the underlying spatial pattern of growth, i.e. growth occurs where the fluorescence is minimized. (B) Spatial distribution of flWGA intensity along the centerline axis of the single cell in (A) averaged across the cross-section and then normalized by the maximum average intensity along the centerline. The time points are indicated with colors progressing from dark red to dark blue. (C) Inset: A typical intensity profile is characterized by one minimum at the septum ($I_{\rm min}$) and two maxima near either pole ($I_{\rm max,1}$, $I_{\rm max,2}$). We define the index of uniformity as $D = 2I_{\rm min}/(I_{\rm max,1} + I_{\rm max,2})$. See Supplementary Information for more details. $D(t)$ is shown for a single cell in (A), revealing a crossover from uniform growth ($\langle D\rangle \simeq 1$) to localized septal growth at $t \sim 50$ min. (D) Ensemble averaged dynamics of the growth uniformity index, $\langle D\rangle$, as a function of time normalized by the division time. Error bars indicate ± 1 standard deviation.

channel and image stacks for stalked cells were acquired every 10 minutes within the fields of view. Fig. 2A shows that the fluorescence intensity is spatially uniform prior to constriction (i.e., for samples at $t < 50$ min), but the flWGA intensity patterns exhibit a pronounced minimum at the septum where the cell-wall is invaginated ($t > 50$ min). In Fig. 2A we present deconvolution processed images obtained using the commercial Huygens software (see Supplementary Methods). The deconvoluted single cell images clearly show the diminished flWGA label in the septal region. Moreover, the 70 and 80 min images even hint at the secondary invaginations in a predivisional cell, consistent with our previous report on intergenerational continuity [2]. For each of these images, Fig. 2B shows the intensity along the centerline axis, averaged over the cell cross-section at each position and then normalized by the maximum value for each time. Because we account for the cross-section, the appearance of the minima in the intensity at the septum is not merely

an artifact of its diminishing width. The spatial distribution of flWGA intensity suggests that growth is spatially uniform for $t < 50$ min and new cell-wall material is primarily synthesized at the invaginations for $t > 50$ min. This septal mode of cell wall growth has been reported earlier with D-amino acid labeling of the cell wall [24, 25], and is also evident in our experiments with synchronized cell wall labeling of *C. crescentus* cells (Supplementary Methods; Supplementary Fig. 11). To quantify the spatial uniformity of cell-wall deposition for each cell in the ensemble we introduce an *intensity uniformity index*, D, given by the ratio of the intensity at the site of the septum ($I_{\min}$) to the mean of the maximum intensities ($I_{\max,1,2}$) on the stalked and swarmer sides of that site (Fig. 2C-inset; Supplementary Information). The intensity uniformity index, D, is close to unity for $t < 50$ min (since $I_{\min} \simeq I_{\max,1,2}$), indicating spatially uniform growth (Fig. 2C). For $t > 50$ min, D dropped sharply to lower values, suggesting that cell wall growth is localized to the septum and is thus coupled to cell wall constriction. Fig. 2D shows the ensemble averaged intensity uniformity index, $\langle D \rangle$, exhibiting a smooth crossover to septal growth for $t > 0.6\tau$.

Relative timer phase prior to cell wall constriction. To relate this observed crossover in cell wall growth to the dynamics of other cell cycle variables, we examined our single cell shape data [2]. We find that the constriction dynamics in individual generations exhibit a biphasic behavior, with an initial period of slow constriction followed by a phase of fast constriction (Figure 3A). We determine the crossover time, t_c, by fitting piecewise exponential curves to the initial and the later phases of decay in $w_{\min}(t)$ (Supplementary Methods and Figures 5A,B). We estimate the onset of constriction by t_c, which has a mean value $t_c = 47 \pm 7$ min at 31°C (Supplementary Figure 5C). The data for $w_{\min}$ across cell lineages collapse to a master crossover curve when time is normalized by interdivision times (Fig. 3B), indicating that a single timescale governs constriction initiation. This crossover dynamic is observed in the analogous data obtained at other temperatures of the medium (Supplementary Figure 6); we find that t_c increases in proportion to τ and κ^{-1} as the temperature is decreased (Supplementary Figure 7). As shown in Figs. 3C, the conditional distributions of the normalized crossover times, t_c/τ, collapse to a single curve for various values of $l(0)$. These observations suggest that the cell cycle phase at the initiation of constriction, t_c/τ, is independent of initial cell length. Indeed our data show that t_c/τ is uncorrelated with the initial cell size (Fig. 3D, red cloud), whereas the cell length at $t = t_c$ increased in proportion to the initial length, $l(t_c) = 1.25\ l(0) + 0.43$ (Fig. 3E, red cloud). By analyzing our shape data at other temperatures we find that t_c/τ remains independent of $l(0)$ (Supplementary Figure 9A), and does

not vary with changing temperature of the growth medium (Supplementary Figure 9B).

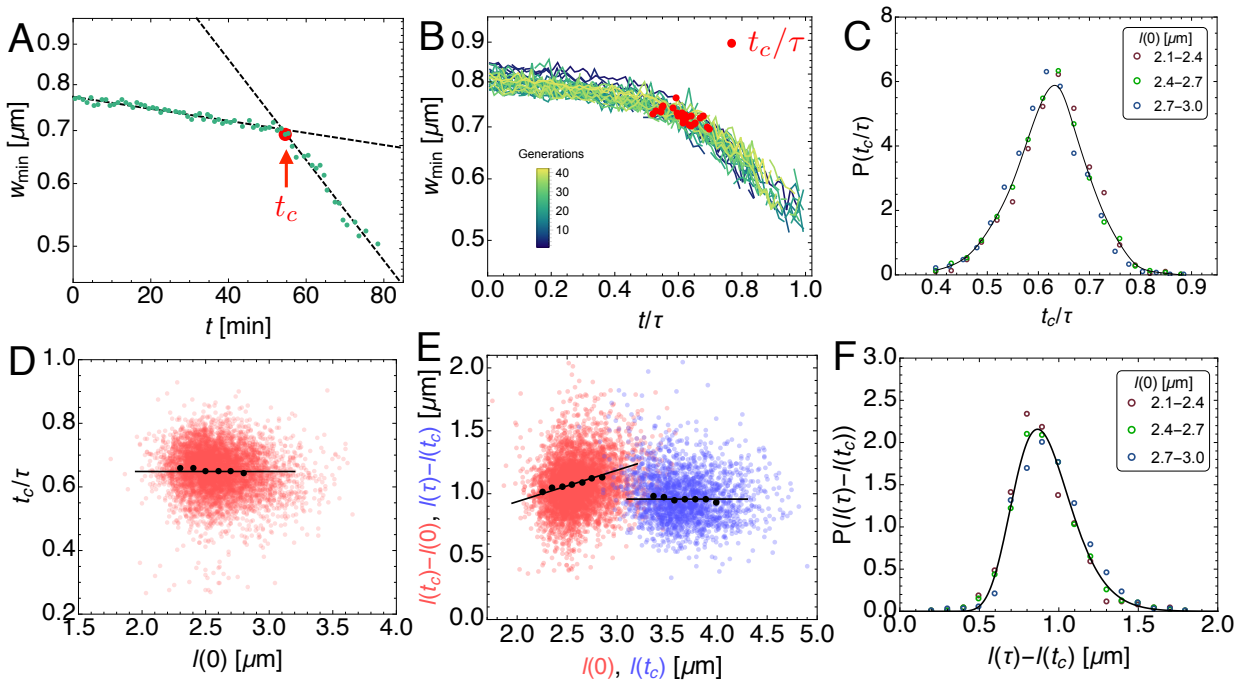

FIG. 3. **Crossover from relative timer to adder-like behavior at the onset of cell wall constriction.** (A) Semi-log plot of the time-dependence of $w_{\min}$ in a typical generation shows two phases of constriction, a slow initial phase followed by a fast constriction phase. We determine t_c by the intersection of the least square exponential fits to the earlier and later portions of the cell cycle (see Supplemental Methods). (B) Dynamics of $w_{\min}$ across generations of a typical cell as functions of the normalized cell cycle time. Locations of t_c/τ are marked by red solid circles. (C) The conditional probability density of the normalized crossover time, t_c/τ, given initial length values, $P(t_c/\tau|l(0))$, shown by colored circles. The density indicates that t_c/τ and $l(0)$ are independent. Solid line is a best fit cubic spline curve. (D) Lack of correlation between t_c/τ and $l(0)$ (red scatter). Black line represent a relative timer: $t_c = 0.63\tau$. The solid circles represent mean data binned in $l(0)$. (E) Positive correlation between the added size before constriction, $l(t_c) - l(0)$ and $l(0)$ (red scatter). The black line represents the best fit: $l(t_c) = 1.25l(0) + 0.43$. Added size for $t > t_c$, is uncorrelated with $l(t_c)$ (blue scatter) supporting a pure adder model during the constriction phase: $l(\tau) = l(t_c) + 0.97$. (F) The conditional probability density of the post-constriction added cell size. Colored circles indicate the ranges of the initial lengths, $l(0)$. The collapse of the distributions indicates the independence of $l(\tau) - l(t_c)$ and $l(0)$. The solid line is a best-fit lognormal distribution.

Pure adder phase during cell wall constriction. While the time to the onset of cell wall constriction is uncorrelated with cell size, the added size in the constriction phase, $\delta' = l(\tau) - l(t_c)$, also showed no correlation with $l(t_c)$ (Fig. 3E, blue cloud). This suggests a *pure adder* mechanism of cell size control for $t_c < t < \tau$, such that the distribution of the added size is independent of

the initial cell length. This adder behavior is indeed confirmed by the collapse of the conditional distributions of the added size $P(\delta'|l(0)\rangle)$ to a single curve, characterized by a log-normal distribution (Fig. 3F) [7]. Furthermore, the time to divide since t_c shows negative correlation with $l(t_c)$ (Supplementary Figure 8). This negative correlation is supported by a model of constant size extension or an *adder* during the constriction phase, $\tau = t_c + \kappa^{-1} \ln\left[1 + \langle\delta'\rangle / l(t_c)\right]$ with $\langle\delta'\rangle = 0.97$ μm. Furthermore, we find that the adder phase post constriction is conserved for all temperatures with a constant mean added size of ~ 1 μm (Supplementary Figures 9 C,D). Since constricting cells primarily grow from the septum (Fig. 2), the added size in the constriction phase is expected to be proportional to the width of the septal plane. Consistent with the model of septal growth, we find that δ' is positively correlated with $w_{\min}(t_c)$ (Supplementary Fig. 10A).

Model for constriction driven by septal growth describes the crossover dynamics. To examine whether septal cell wall synthesis in exponentially elongating cells (Fig. 2) can reproduce the observed crossover dynamics of constriction (Fig. 3), we consider a quantitative model for cell wall constriction driven by septal growth [21]. We assume that the shape of the constriction zone is given by two intersecting hemispherical segments with diameter w, and constriction proceeds by completing the missing parts of the hemispheres while maintaining the curvature of the preformed spherical segments. The total surface area of the septum is given by $S(t) = \pi w l_s(t)$, where $l_s(t)$ is the total length of the hemispherical segments (Fig. 4A). Since constriction proceeds concomitantly with longitudinal growth [2], exponential growth of septal surface area implies:

$$\frac{dl_s}{dt} = \kappa l_s + v_0 \,, \tag{2}$$

where v_0 is the speed of septum synthesis at $t = 0$, which we determine by fitting our model to the data for $w_{\min}(t)$. The solution to Eq. (2) can then be used to derive the time-dependence of $w_{\min}(t) = \sqrt{w^2 - l_s(t)^2}$. Using the initial condition, $l_s(0) = 0$, we derive a simple relation

$$w_{\min}(t)/w_{\min}(0) = \sqrt{1 - \left(l_0/w_{\min}(0)\right)^2 \left(e^{\kappa t} - 1\right)^2} \,,$$

between the rescaled width and the rescaled time variable (κt), where $l_0 = v_0 \kappa^{-1}$. The dynamics of constriction are then solely controlled by the dimensionless parameter $l_0/w_{\min}(0)$, and exhibits a crossover point (Fig. 4B), which we determine analytically following the procedure in Fig. 3 (Supplementary Methods). As shown in Fig. 4B (inset), the model prediction for the crossover time is in excellent agreement with the mean crossover time in our experimental data ($\langle\kappa t_c\rangle = 0.37$, Fig. 4B), and the time to the onset of fast constriction is insensitive to variations in $l_0/w_{\min}(0)$.

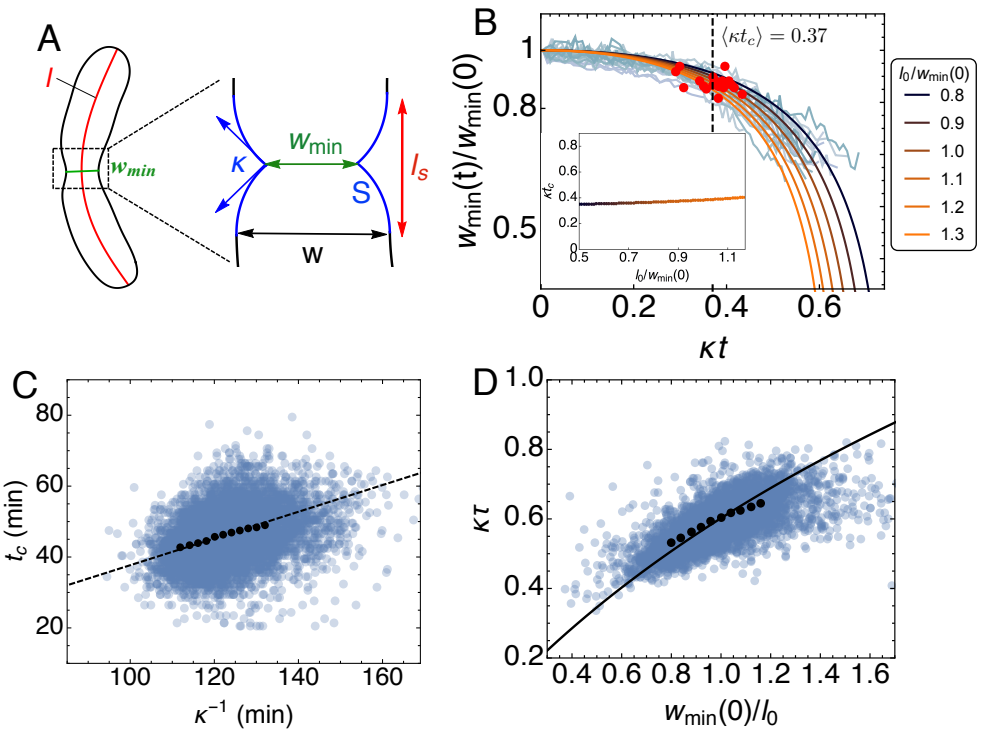

FIG. 4. **Septal growth model predicts the onset of cell wall constriction and interdivision times.** (A) A representative splined contour of a *C. crescentus* cell, illustrating the shape parameters, l (red) and $w_{\min}$ (green). The region inside the dashed rectangle represents the constriction zone, where S is the surface area of the septal cell-wall (blue) synthesized after constriction. (B) Dynamics of the width of the pinch-off plane (normalized by $w_{\min}(0)$), with time normalized by κ^{-1}. Predictions of the septal growth model are shown by solid curves at various values of the dimensionless parameter, $l_0/w_{\min}(0)$. Experimental data for different generations of a representative cell are shown in light blue with the locations of the crossover marked by solid red circles. Inset: No dependence of the crossover time (normalized by κ^{-1}) on $l_0/w_{\min}(0)$, as predicted by the theoretical model. (C) Positive correlation between t_c and κ^{-1}. The solid circles represent mean data binned in κ^{-1} and the dashed line represents the best fit curve $t_c = 0.37\kappa^{-1}$. (D) Normalized interdivision times ($\kappa\tau$) vs the normalized initial width of the pinch-off plane (binned data in solid circles; model prediction, Eq. (3), in solid curve).

This implies that t_c is regulated by the longitudinal growth rate κ, which is consistent with the observed positive correlation between t_c and κ^{-1} (Fig. 4C).

Another prediction of the constriction model is that the interdivision times increase with $w_{\min}(0)/l_0$, because the wider cells require more material to close the septum. Based on our model, we predict a simple relation between the interdivision times and the initial width of the

constriction plane,

$$\tau = \kappa^{-1} \ln \left(1 + \frac{\Delta w_{\min}}{l_0} \right), \tag{3}$$

where, $\Delta w_{\min} = \sqrt{w_{\min}(0)^2 - w_{\min}(\tau)^2}$. Thus, the interdivision time is predicted to be larger for cells with larger septum width, $\Delta w_{\min}$. We find a positive correlation in our data between $\kappa\tau$ and $w_{\min}(0)/l_0$, and the mean trend in our data is in good quantitative agreement with our model with no fitting parameters (Fig. 4D). Furthermore, Eqs. (1) and (3) together imply a negative correlation between initial septal width, $w_{\min}(0)$, and the cell size at division, $l(\tau)$, which is in quantitative agreement with our data (Supplementary Figure 10B).

In summary, the septal growth model allows us to derive two key conclusions, supported by our data. First, the time to the onset of constriction (t_c) is controlled by the growth rate (κ). Second, the interdivision times are larger for cells with larger initial septal width.

DISCUSSION

The adder phase of cell-wall growth ($t > t_c$) coupled with relative size thresholding prior to constriction ($t < t_c$) comprise a biphasic growth model for *C. crescentus* cells. This mechanism is illustrated using the schematic in Fig. 5. Newborn cells exhibit lateral elongation with uniform patterning of cell wall synthesis prior to constriction ($t < t_c$). Cells begin their constriction at a fixed phase in the cell cycle. During the constriction phase, i.e. for $t > t_c$, cells primarily add new cell wall material at the septum. This phase of growth is characterized by a constant cell size extension, which is related to the cell width. The length added after $t > t_c$ originates primarily from the surface area (or radius) of the daughter cell poles. Taken together, the crossover from uniform cell wall growth to localized septal growth provides a physical basis for a *mixer model* of cell size control.

Like the adder model, the mixer model automatically ensures cell size homeostasis: with each division, the cell length regresses to the ensemble average [16, 26], $\delta r/(1 - ar)$, where r is the mean ratio of the daughter to the mother cell size (length). It is interesting to consider why *E. coli* exhibits a pure adder behavior while *C. crescentus* exhibits a mixer behavior. One notable difference between the species is that *E. coli* can initiate multiple rounds of DNA replication per cell cycle while *C. crescentus* has a strict one-to-one correspondence between these processes. While the molecular mechanism for the control of the onset of cell wall constriction is unknown, it is likely that the first timer phase is related to the duration of chromosome replication, which is independent

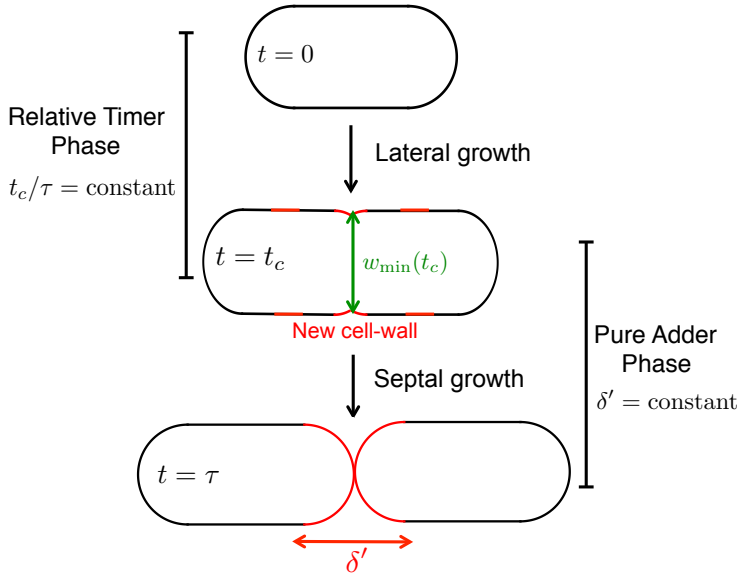

FIG. 5. **Mixer mechanism for cell wall growth.** A schematic of the mixer model for spatiotemporal coordination of cell wall growth in *C. crescentus* cells. Growth is spatially uniform for $t < t_c$ when cell wall deposition occurs laterally along the entire cell length except the poles (red). For $t > t_c$, cell wall growth is dominated by septal cell wall synthesis that leads to constant size extension determined by the surface area of the new poles (red).

of cell size. Alternatively, it has been suggested that nutrient uptake imposes condition-dependent constraints on surface-area-to-volume ratios and in turn the growth mechanism [17]. While cell cycle checkpoints have so far not been quantitatively established for bacteria, our study provides a crucial insight for further investigation into the molecular candidates regulating cell size and division control in bacteria.

REFERENCES

[1] Iyer-Biswas, S. *et al.* Scaling laws governing stochastic growth and division of single bacterial cells. *Proceedings of the National Academy of Sciences* **111**, 15912–15917 (2014).

[2] Wright, C. S. *et al.* Intergenerational continuity of cell shape dynamics in caulobacter crescentus. *Scientific Reports* **5**, 9155 (2015).

[3] Wang, P. *et al.* Robust growth of escherichia coli. *Current Biology* **20**, 1099–1103 (2010).

[4] Campos, M. *et al.* A constant size extension drives bacterial cell size homeostasis. *Cell* **159**, 1433–1446 (2014).

[5] Taheri-Araghi, S. *et al.* Cell-size control and homeostasis in bacteria. *Current Biology* **25**, 385–391 (2015).

[6] Sauls, J. T., Li, D. & Jun, S. Adder and a coarse-grained approach to cell size homeostasis in bacteria. *Current opinion in cell biology* **38**, 38–44 (2016).

[7] Amir, A. Cell size regulation in bacteria. *Physical Review Letters* **112**, 208102 (2014).

[8] Deforet, M., van Ditmarsch, D. & Xavier, J. B. Cell-size homeostasis and the incremental rule in a bacterial pathogen. *Biophysical Journal* **109**, 521–528 (2015).

[9] Soifer, I., Robert, L. & Amir, A. Single-cell analysis of growth in budding yeast and bacteria reveals a common size regulation strategy. *Current Biology* (2016).

[10] Donachie, W. Relationship between cell size and time of initiation of dna replication. *Nature* **219**, 1077–1079 (1968).

[11] Koppes, L., Meyer, M., Oonk, H., De Jong, M. & Nanninga, N. Correlation between size and age at different events in the cell division cycle of escherichia coli. *Journal of Bacteriology* **143**, 1241–1252 (1980).

[12] Osella, M., Nugent, E. & Lagomarsino, M. C. Concerted control of escherichia coli cell division. *Proceedings of the National Academy of Sciences* **111**, 3431–3435 (2014).

[13] Tanouchi, Y. *et al.* A noisy linear map underlies oscillations in cell size and gene expression in bacteria. *Nature* **523**, 357–360 (2015).

[14] Donachie, W., Begg, K. & Vicente, M. Cell length, cell growth and cell division. *Nature* **264**, 328–333 (1976).

[15] Kubitschek, H. Bilinear cell growth of escherichia coli. *Journal of Bacteriology* **148**, 730–733 (1981).

[16] Jun, S. & Taheri-Araghi, S. Cell-size maintenance: universal strategy revealed. *Trends in Microbiology* **23**, 4–6 (2015).

[17] Harris, L. K. & Theriot, J. A. Relative rates of surface and volume synthesis set bacterial cell size. *Cell* **165**, 1479–1492 (2016).

[18] Wang, J. D. & Levin, P. A. Metabolism, cell growth and the bacterial cell cycle. *Nature Reviews Microbiology* **7**, 822–827 (2009).

[19] Mitchison, J. M. *The biology of the cell cycle* (CUP Archive, 1971).

[20] Marshall, W. F. *et al.* What determines cell size? *BMC Biology* **10**, 101 (2012).

[21] Banerjee, S., Scherer, N. F. & Dinner, A. R. Shape dynamics of growing cell walls. *Soft Matter* **12**, 3442–3450 (2016).

[22] Lin, Y., Li, Y., Crosson, S., Dinner, A. R. & Scherer, N. F. Phase resetting reveals network dynamics underlying a bacterial cell cycle. *PLoS Comput Biol* **8**, e1002778 (2012).

[23] Ursell, T. S. *et al.* Rod-like bacterial shape is maintained by feedback between cell curvature and cytoskeletal localization. *Proceedings of the National Academy of Sciences* **111**, E1025–E1034 (2014).

[24] Aaron, M. *et al.* The tubulin homologue ftsz contributes to cell elongation by guiding cell wall precursor synthesis in caulobacter crescentus. *Molecular Microbiology* **64**, 938–952 (2007).

[25] Kuru, E. *et al.* In situ probing of newly synthesized peptidoglycan in live bacteria with fluorescent d-amino acids. *Angewandte Chemie International Edition* **51**, 12519–12523 (2012).

[26] Voorn, W., Koppes, L. & Grover, N. Mathematics of cell division in escherichia coli. *Curr. Top. Mol. Genet* **1**, 187–194 (1993).

ACKNOWLEDGEMENTS

We thank Charles Wright and Srividya Iyer-Biswas for measurements and shape analysis of *C. crescentus* single cell data [1, 2]. We gratefully acknowledge funding from the NSF Physics of Living Systems (NSF PHY-1305542), the NSF Materials Research Science and Engineering Center (MRSEC) at the University of Chicago (NSF DMR-0828854), the W. M. Keck Foundation and the Graduate Program in Biophysical Sciences at the University of Chicago (T32 EB009412/EB/NIBIB NIH HHS/United States). SB acknowledges support from University College London for completion of part of this work. We thank Sean Crosson and Aretha Fiebig for contributing reagents, materials and helpful discussions.

AUTHOR CONTRIBUTIONS

S.B., K.L., A.R.D. and N.F.S. designed research; S.B., K.L., A.S., M.D. and T.K. performed research; S.B., A.R.D. and N.F.S. wrote the manuscript.

COMPETING FINANCIAL INTERESTS

The authors declare no competing financial interests.